Thermochimica Acta, 211 (1992) 137–153
Elsevier Science Publishers B.V., Amsterdam

Non-isothermal crystallization kinetics of *n*-paraffins with chain lengths between thirty and fifty

Ahmed Hammami and Anil K. Mehrotra

Department of Chemical and Petroleum Engineering, The University of Calgary, Calgary, AB T2N 1N4 (Canada)

(Received 3 April 1992)

Abstract

The non-isothermal crystallization kinetics of four high-purity even-number *n*-paraffins, namely *n*-$C_{30}H_{62}$, *n*-$C_{34}H_{70}$, *n*-$C_{44}H_{90}$ and *n*-$C_{50}H_{102}$, have been studied using differential scanning calorimetry (DSC). The data are treated in terms of the Ozawa theory utilizing, for the first time, a semi-empirical formulation for the so-called Ozawa cooling crystallization function. The derivations are based on the theories of surface nucleation and growth rate of extended-chain crystals. Predictions from the proposed model are in excellent agreement with the experimental data for the four *n*-paraffins at relatively low supercooling.

INTRODUCTION

Most crude oils consist of various fractions of heavy hydrocarbons, which are known to precipitate at low temperatures as paraffin deposits. Accumulation of these solids in transport pipes and process equipment is an old and expensive problem in the petroleum industry. A vital step towards treating this problem is to be able to predict the onset of wax crystallization, i.e. the wax appearance point, as well as the total amount of paraffin wax deposited under given processing conditions.

Typically, an average crude paraffin wax consists of long molecules with chain lengths between twenty-six and fifty [1]. The modelling of the solidification process for such a mixture is therefore contingent upon the knowledge of the crystallization behaviour of its major components. In the present work, the crystallization kinetics of four even-number *n*-paraffins of very high purity is undertaken.

The Ozawa theory [2] for non-isothermal crystallization is adopted to describe the crystallization of pure *n*-paraffins at constant cooling rates. This theory makes it possible to predict not only the type of nucleation

Correspondence to: A.K. Mehrotra, Department of Chemical and Petroleum Engineering, The University of Calgary, Calgary, AB T2N 1N4, Canada.

involved during crystallization but also the morphology of the grown crystals. In addition, a semi-empirical formulation for the Ozawa cooling crystallization function is proposed to model the non-isothermal crystallization data successfully.

THEORETICAL

Ozawa's theory

Ozawa [2] has extended the Avrami theory [3] for isothermal crystallization to the non-isothermal situation, assuming that the sample is heated or cooled at a constant rate and the mathematical derivation of Evans [4] is valid. Accordingly, the degree of phase transformation $X(T)$ at temperature T and cooling rate λ is given by

$$X(T) = 1 - \exp\left(\frac{-K(T)}{|\lambda|^n}\right) \tag{1}$$

where $K(T)$ is termed the cooling crystallization function, and n is the Ozawa index (also known as the Avrami exponent) which depends on the type of nucleation and the growth dimensions. The theoretical values of n for various crystallization mechanisms are listed in Table 1.

By taking the logarithm of both sides of eqn. (1) twice at constant temperature, we get

$$\ln[-\ln(1 - X(T))] = \ln(K(T)) + n \ln|\lambda|^{-1} \tag{2}$$

As written, eqn. (2) allows the determination of the Ozawa index in terms of the cooling rate and the fraction of crystallized material. Theoretically, a plot of $\ln[-\ln(1 - X(T))]$ versus $\ln|\lambda|^{-1}$ is linear with n being the slope

TABLE 1

Theoretical values of n and the isothermal rate constant k for different morphologies and nucleation mechanisms [5]

Crystal growth	Nucleation mode	Avrami exponent (n)	Isothermal rate constant [a] (k)
Rod	Heterogeneous	1	NGA
	Homogeneous	2	$\dot{N}GA/2$
Disc	Heterogeneous	2	$\pi G^2 ND$
	Homogeneous	3	$(\pi/3)G^2\dot{N}D$
Sphere	Heterogeneous	3	$(4\pi/3)NG^3$
	Homogeneous	4	$(\pi/3)\dot{N}G^3$

[a] A is constant area, D is thickness, G is linear growth rate, N is nucleation density and $\dot{N}$ is nucleation rate.

and $\ln[K(T)]$ being the intercept. Alternatively, the cooling crystallization function can be evaluated from the half crystallization temperature $T_{1/2}$ (the temperature at which 50% phase conversion is achieved)

$$K(T_{1/2}) = \ln(2)\,|\lambda|^n \tag{3}$$

In his derivation of eqn. (1), Ozawa has neglected two factors, namely the slow secondary crystallization and the fold length of the polymer chain. However, because the crystallization process proceeds under non-isothermal conditions, the slow secondary crystallization would be virtually absent as the temperature decreases continuously [6]. The fold length effects are also irrelevant for this study because, unlike polymers, *n*-paraffins do not crystallize by chain folding unless their chain-lengths are longer than or equal to $C_{150}H_{302}$ [7]. The shorter *n*-paraffins, like those studied here, would crystallize in the lamellar chain-extended mode [8, 9].

Formulation of the cooling crystallization function K(T)

Ozawa [2] has shown that, in the case of homogeneous nucleation, the cooling crystallization function $K(T)$ is expressed as

$$K(T) = g\int_{T_m^\circ}^{T} \dot{N}(\theta)[U(T) - U(\theta)]^m G(\theta)\,\mathrm{d}\theta \tag{4}$$

where g is a geometric factor, n equals $m+2$, $\dot{N}(\theta)$ is the nucleation density rate i.e. the nuclei appear at a constant rate per unit volume activated between temperatures T_m° and θ, T_m° is the equilibrium melting temperature, $G(\theta)$ is the crystal growth rate at temperature θ, and $U(T)$ is related to $G(\theta)$ through

$$U(T) = \int_{T_m^\circ}^{T} G(\theta)\,\mathrm{d}\theta \tag{5}$$

In the case of heterogeneous nucleation, the cooling crystallization function maintains the general form of eqn. (4) with the exception that n becomes equal to $m+1$, and the nucleation density is constant. In any case, $K(T)$ is clearly a complicated function of nucleation and growth rates; the need to resort to a semi-empirical formulation is thus necessary.

If a sample is cooled from a temperature above T_m°, then crystallization will not start until $T \leq T_m^\circ$. Therefore, the constant cooling rate λ is given by

$$|\lambda| = \left|\frac{\mathrm{d}T}{\mathrm{d}t}\right| = \left|\frac{\Delta T}{\Delta t}\right| = \frac{T_m^\circ - T}{t} \tag{6}$$

where t denotes the time required to cool the sample from T_m° to T, and

ΔT is the degree of undercooling. Let $\Gamma(T)$ be defined as

$$\Gamma(T) = \frac{K(T)}{|\lambda|^n} \tag{7}$$

It follows that

$$\Gamma(T) = \left[\frac{K(T)}{(\Delta T)^n}\right] t^n = \Psi(T) t^n \tag{8}$$

where $\Psi(T)$ denotes the ratio of $K(T)$ to $(\Delta T)^n$. Substituting eqn. (8) into eqn. (1) gives

$$X(T) = 1 - \exp[-\Psi(T) t^n] \tag{9}$$

Equation (9) is similar in form to the well-known Avrami equation for isothermal crystallization which reads [3]

$$X(T) = 1 - \exp(-kt^n) \tag{10}$$

where k is the overall isothermal rate constant and n is the Avrami exponent. The theoretically derived expressions for k with different crystallization mechanisms are reported in Table 1. The similarities between eqns. (9) and (10) support the argument that the cooling crystallization function is related to the overall rate of crystallization [6].

To formulate $\Psi(T)$, and hence $K(T)$, explicitly as a function of temperature, we have assumed that $\Psi(T)$ has the same temperature dependence as k, that the crystallization is overwhelmingly homogeneous, and that the formed crystals are one-dimensional. According to Table 1, these assumptions lead to

$$k(T) = \frac{A}{2} G(T) \dot{N}(T) \tag{11}$$

and hence

$$\Psi(T) \approx G(T) \dot{N}(T) \tag{12}$$

where $\dot{N}(T)$ is the rate of nucleation density and $G(T)$ is the growth rate. The dependence of $\dot{N}(T)$ and $G(T)$ on the crystallization temperature and on the supercooling ΔT can be described by the homogeneous nucleation theory [10–12] and the Hoffman growth-rate theory for extended-chain crystals [13], respectively.

For a homogeneous nucleation process, Turnbull and Fisher [10] have shown that the nucleation frequency amounts to

$$\dot{N}(T) = N_0 \exp\left(\frac{-E_a}{\kappa T}\right) \exp\left(\frac{-\Delta G^*}{\kappa T}\right) \tag{13}$$

where N_0 is a slightly temperature-dependent factor, κ is the Boltzman constant, E_a is the activation energy for motion across the nucleus–liquid interface, and ΔG^* is the change in free energy to form a crystal nucleus of critical size. Equation (13) allows the temperature dependence of the crystal nucleation rate to be understood in terms of two competing processes. Opposing one another are the driving force for nucleation, which increases with decreasing temperature, and the rate of molecular transport (diffusion) in the melt, which decreases with decreasing temperature.

The formulation of ΔG^* is strongly dependent on the geometry of the critical nucleus (sphere, plate, rod, etc.). For the case of a cylindrical nucleus of variable length and radius, ΔG^* is defined as [14]

$$\Delta G^* = \frac{8\pi\sigma^2\sigma_e(T_m^\circ)^2}{(\Delta H_f \Delta T)^2} \tag{14}$$

where ΔH_f is the latent heat of fusion for 100% crystalline material, and σ and σ_e are the lateral and end surface free energies, respectively.

For the specific case of extended-chain crystallization of monodisperse flexible chains, Hoffman [13] derived the expression for the growth rate

$$G(T) = M_0 b\beta \exp\left[\frac{-(2bl\sigma + 2ab\sigma_e)}{\kappa T}\right]\left\{1 - \exp\left[\frac{-(abl\Delta H_f)}{T_m^\circ \kappa T}(T_0 - T)\right]\right\} \tag{15}$$

where M_0 is the number of reacting species, β is the diffusion term, a and b are lateral chain dimensions, l is the chain length, T_0 the highest temperature for finite rate of growth (T_0 being very close to T_m° for extended chains) and the other terms are as defined earlier. For relatively low effective supercooling ($T_0 - T$), the last exponential term can be expanded to yield

$$G(T) = K'(T_0 - T) \approx G_0 \Delta T \tag{16}$$

where the prefactors K' and/or G_0 are presumed to be not strongly temperature dependent.

Because at relatively low supercoolings the crystallization process is essentially nucleation controlled, the pre-exponential transport (diffusion) terms in eqns. (13) and (15) have minor effects [13] and, hence, can be assumed constant. For instance, the ratio $E_a/\kappa T$ is reported to be in the vicinity of 5.5 for the n-alkanes at the melting temperature [11]. Consequently, the combination of eqns. (12)–(14), and (16) leads to

$$\Psi(T) = C_1 \Delta T \exp\left(\frac{-C_2}{T(\Delta T)^2}\right) \tag{17}$$

where all the prefactors, including N_0 and G_0, have been combined in C_1, the parameter C_2 is associated with the free energy of nucleation.

Dividing both sides of eqn. (17) by ΔT and taking the logarithm yields

$$\ln[\Psi^*(T)] = \ln(C_1) - \frac{C_2}{T(\Delta T)^2} \tag{18}$$

where $\Psi^*(T)$ equals $\Psi(T)/\Delta T$, i.e. $K(T)/(\Delta T)^{n+1}$. For eqn. (18) to be valid, the experimental results should yield a straight line when $\ln[\Psi^*(T)]$ is plotted against $1/T(\Delta T)^2$.

EXPERIMENTAL

Materials and sample preparation

Four even-number *n*-paraffins of high purity with chain lengths between thirty and fifty were purchased from Aldrich Chemical Co., Milwaukee, WI (USA). The purities of these compounds are listed in Table 2. All four *n*-paraffins are white powders.

About 4–8 mg of each of these compounds were weighed and carefully distributed over the crucible (sample container) base to ensure a good thermal contact between the specimen and the calorimeter; the crucibles were then cold-welded to their covers using a mechanical crucible sealer.

TABLE 2

Purites and equilibrium melting temperatures for the even-number *n*-paraffins

Compound	Purity	Measured T_m° (°C)
n-Triacontane (*n*-$C_{30}H_{62}$)	99%	67.7
n-Tetratriacontane (*n*-$C_{34}H_{70}$)	98%	74.3
n-Tetratetracontane (*n*-$C_{44}H_{90}$)	99%	87.7
n-Pentacontane (*n*-$C_{50}H_{102}$)	>99%	93.7

Instrumentation

The work described in this study was carried out using a Mettler differential scanning calorimeter Model DSC-12E. The sample chamber was continuously purged with dry nitrogen. In this calorimeter, it is possible to melt and recrystallize the same *n*-paraffin specimen many times without apparent thermal degradation. Thus, the same sample can be used for a whole series of runs, which improves the reproducibility of DSC measurements. The DSC-12E calorimeter was calibrated for temperature using pure indium ($T_m^\circ = 156.6$°C).

The non-isothermal crystallization was performed at constant cooling rates in the range of 1–10°C min^{-1}. Before being cooled at a program-

mable rate, each sample was held initially at 125°C for at least 2 min so as to destroy all traces of crystallinity present. The relative crystallinity which developed between T_m° and T was defined as the fractional area confined between the rate-temperature curve and the baseline of the measured DSC exotherm [15]. The temperatures were corrected for a small thermal lag between the sample and the calorimeter furnace using a calibration technique using pure indium [16].

The equilibrium melting temperatures of the *n*-paraffins, reported in Table 2, were evaluated from the 1°C min^{-1} melting scans. These values do not correspond to the peak melting temperatures but rather to the return to the baseline temperatures [17]. For instance, as correctly pointed out by Phillips and Campbell [17], the peak melting temperatures are often broad and not as reproducible as those of the return to the baseline.

RESULTS AND DISCUSSION

Some representative crystallization exotherms of n-$C_{50}H_{102}$ at three cooling rates are shown in Fig. 1. The actual cooling curves for such a compound are too numerous to show and so only those measured at 1, 5 and 10°C min^{-1} are presented. As can be seen, the baseline is the continuation of the straight lines observed on the DSC thermograms before and after completion of the evolution of crystallization heat. The data treatment, then, involves calculating the relative crystallinity as a function of temperature using [15]

$$\frac{X(T)}{X_{inf}} = \int_{T_a}^{t} \left(\frac{dH}{dT}\right) dT \Big/ \int_{T_a}^{T_c} \left(\frac{dH}{dT}\right) dT \tag{19}$$

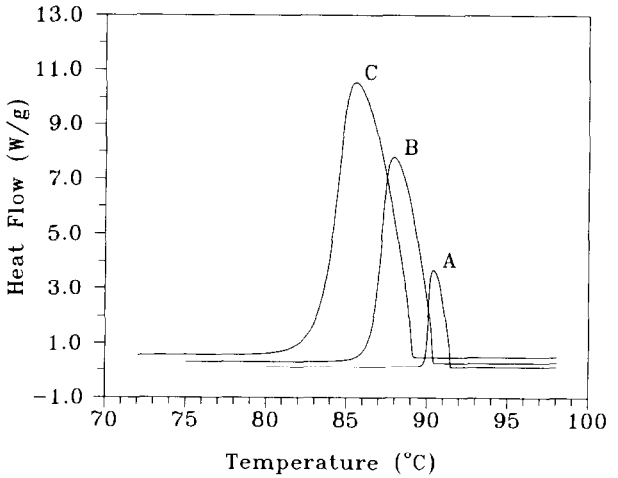

Fig. 1. Typical DSC crystallization exotherms of n-$C_{50}H_{102}$ at different cooling rates: curve A, 1°C min^{-1}; curve B, 5°C min^{-1}; curve C, 10°C min^{-1}.

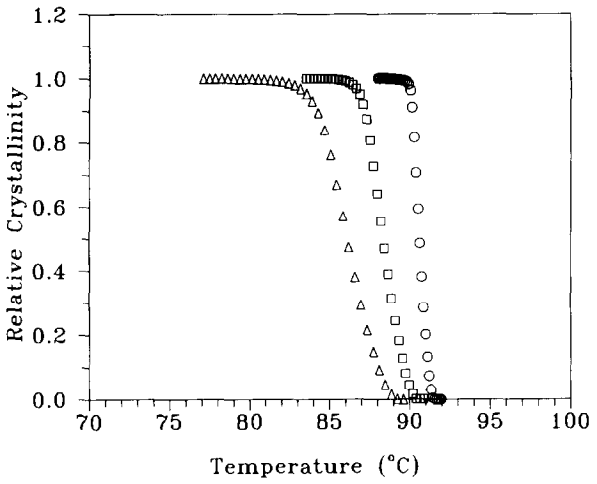

Fig. 2. Plot of relative crystallinity as a function of temperature for n-$C_{50}H_{102}$ at different cooling rates: ○, 1°C min^{-1}; □, 5°C min^{-1}; △, 10°C min^{-1}.

where X_{inf} is the crystallinity at the termination of the crystallization process, and T_s and T_e are the onset and end temperatures of crystallization, respectively. Figure 2 shows the calculated relative crystallinity values that correspond to the cooling exotherms of Fig. 1. An important characteristic of Fig. 2 is the shape of the curves. All the curves of relative crystallinity versus temperature have nearly the same shape. This would indicate that only the retardation effects of cooling rate on crystallization are observed for these curves.

Apart from shifts along the temperature scale and variation in the magnitude of the heat flow, the DSC thermograms for n-$C_{44}H_{90}$ were found to be similar to those for n-$C_{50}H_{102}$. In Fig. 3, however, the DSC exotherms of n-$C_{34}H_{70}$ show two peaks at all cooling rates. Similar results were obtained with n-$C_{30}H_{62}$. The only difference, however, is that no sharp spikes like those shown in Fig. 3 were observed for n-$C_{30}H_{62}$ at any cooling rate. These marked shoulders may be caused by the crystallization of a small fraction of different n-paraffins which may be present in n-$C_{34}H_{70}$ in the form of impurities [9].

The double-peak feature is a clear indication of the presence of a solid–solid transition for such compounds. Solid–solid transitions have been investigated extensively in the literature [18–21], where it is shown that n-paraffins with chain lengths between twenty and thirty-six exhibit transition points in the solid state. The transition often involves a rotational motion at the molecular level from the rotator solid phase α to the denser, low-temperature, non-rotating solid phase β.

The solid–solid transition observed during crystallization of the shorter n-paraffins complicates the determination of the relative crystallinity

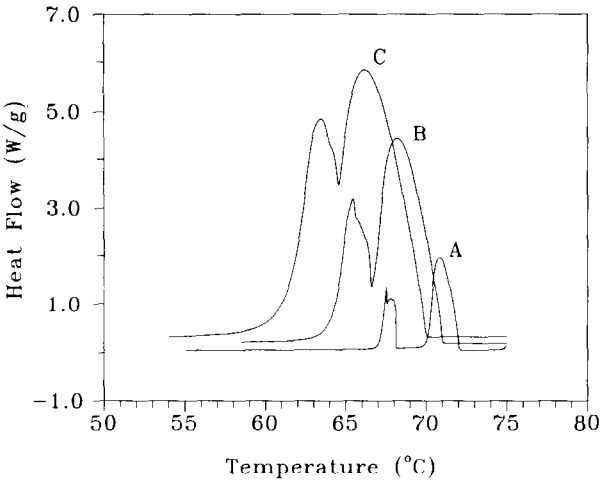

Fig. 3. Typical DSC crystallization exotherms of n-$C_{34}H_{70}$ at different cooling rates: curve A, 1°C min^{-1}; curve B, 5°C min^{-1}; curve C, 10°C min^{-1}.

values. As depicted in Fig. 3, the two peaks do not separate enough for the trace to return to the baseline except at very low cooling rates. To overcome this problem, we have resolved the double peak in each thermogram into two separate exotherms, α and β, as shown in Fig. 4. The procedure involves rescaling the completely resolved α peak, i.e. the one measured at 1°C min^{-1}, and superimposing it on those which correspond to the higher cooling rate exotherms. Evidently, the onset of crystallization occurs within the high temperature α peak and so only such an exotherm is considered for analyses in the present work.

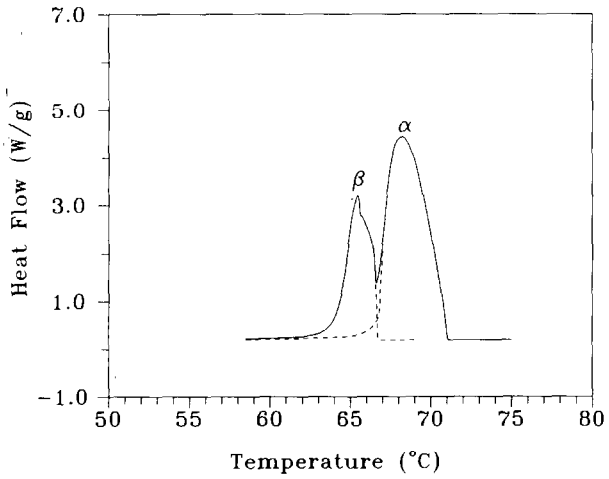

Fig. 4. Extrapolation of the α and β peaks for n-$C_{34}H_{70}$: cooling rate 5°C min^{-1} (same as curve B in Fig. 3).

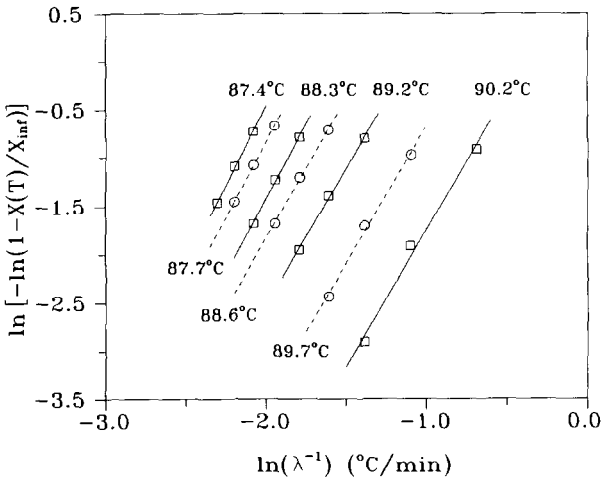

Fig. 5. Plot of $\ln[-\ln(1-X(T)/X_{inf})]$ vs. $\ln(\lambda^{-1})$ for the non-isothermal crystallization of n-$C_{50}H_{102}$ at different temperatures.

Figures 5–8 present plots representative of the Ozawa equation, eqn. (2), for n-$C_{50}H_{102}$, n-$C_{44}H_{90}$, n-$C_{34}H_{70}$ and n-$C_{30}H_{62}$, that is, plots of $\ln[-\ln(1-X(T)/X_{inf}]$ versus $\ln|\lambda^{-1}|$ at constant temperature. If eqn. (2) is valid, the curves corresponding to a given temperature must be a straight line, with the slope being the Avrami exponent. Indeed, Figs. 5–8 show good agreement between experimental results and theoretical predictions. However, the use of eqn. (2) requires values of relative crystallinity at a given temperature for different cooling rates. To cover the widest possible range of temperatures, we have applied eqn. (2) to all

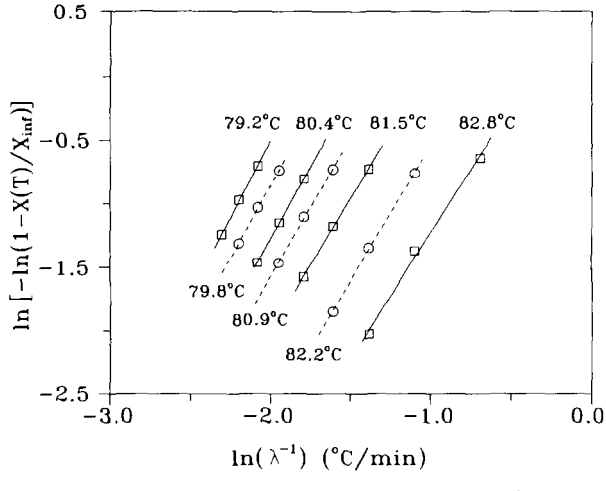

Fig. 6. Plot of $\ln[-\ln(1-X(T)/X_{inf})]$ vs. $\ln(\lambda^{-1})$ for the non-isothermal crystallization of n-$C_{44}H_{90}$ at different temperatures.

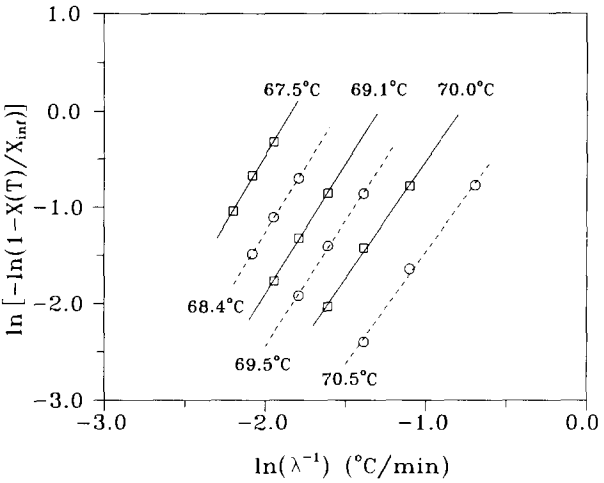

Fig. 7. Plot of $\ln[-\ln(1-X(T)/X_{inf})]$ vs. $\ln(\lambda^{-1})$ for the non-isothermal crystallization of n-$C_{34}H_{70}$ at different temperatures.

the experimental cooling curves considering three consecutive cooling rates at a time.

In the present work, the determination of the Avrami exponent was made for the relative crystallinity data lower than 0.5. The use of higher fractions, where the effects of impingement and distortion of the growing crystals are quite significant, can lead to erroneous low values of n [6]. The values of the Avrami exponent determined by this method are listed in Table 3 as a function of temperature. In general, the Avrami exponent has values between 2 and 3 which correspond to needle and plate

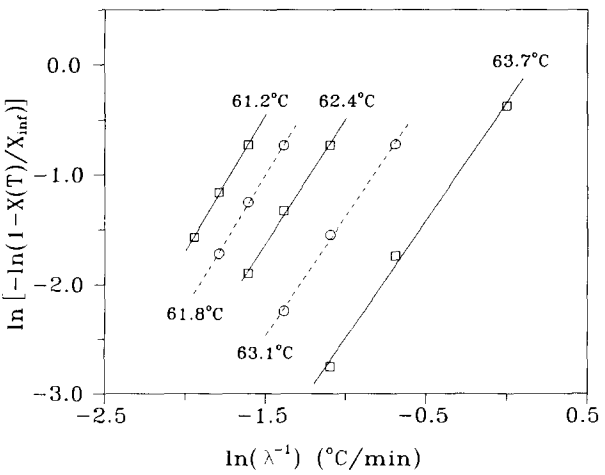

Fig. 8. Plot of $\ln[-\ln(1-X(T)/X_{inf}]$ vs. $\ln(\lambda^{-1})$ for the non-isothermal crystallization of n-$C_{30}H_{62}$ at different temperatures.

TABLE 3

Avrami exponents as a function of temperature for the four *n*-paraffins

n-$C_{30}H_{62}$		n-$C_{34}H_{70}$		n-$C_{44}H_{90}$		n-$C_{50}H_{102}$	
T (°C)	n	T (°C)	n	T (°C)	n	T (°C)	n
61.2	2.4	67.5	2.7	79.2	2.3	87.4	3.2
61.8	2.4	68.4	2.7	79.8	2.3	87.7	3.1
62.4	2.3	69.1	2.7	80.4	2.3	88.3	3.1
63.1	2.2	69.5	2.6	80.9	2.2	88.6	2.9
63.7	2.2	70.0	2.5	81.5	2.1	89.2	2.8
–	–	70.5	2.4	82.2	2.1	89.7	2.8
–	–	–	–	82.8	2.1	90.2	2.8

morphologies, respectively. These findings are expected, because *n*-paraffins are reported to crystallize into shapes most frequently described as plates, needles and malcrystalline masses [22–24]. In particular, crystals grown from highly concentrated solutions or the melt usually contain many imperfections; bent and twisted plates, needles attached to plates, and other evidences of malcrystallinity are observed [25].

The Avrami exponents reported in Table 3 show a slight temperature dependence; they seem to decrease with increasing temperature. A possible explanation of such a phenomenon is that, due to the non-isothermal nature of the experiment, the overall crystallization rate would increase as the temperature is lowered. If nuclei are not randomly distributed in the melt, then impingement effects may occur regardless of

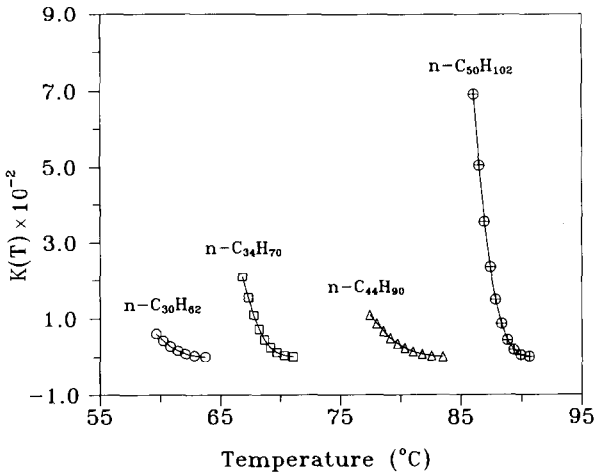

Fig. 9. Temperature dependence of the Ozawa cooling crystallization function for the four *n*-paraffins.

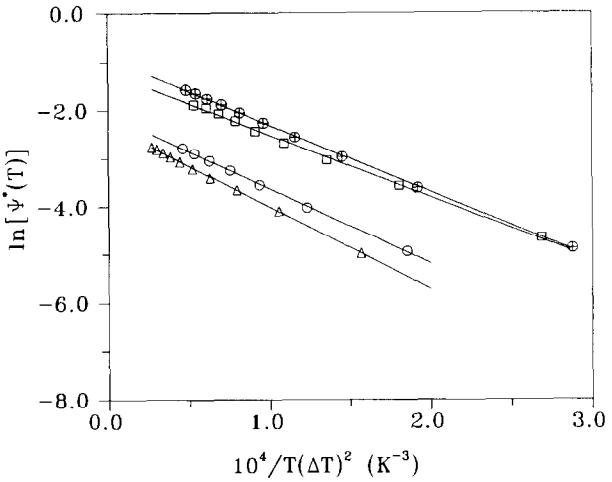

Fig. 10. Plots of $\ln[\Psi^*(T)]$ vs. $1/T(\Delta T)^2$ for the four n-paraffins (symbols as in Fig. 9).

whether the crystalline fraction is smaller than 0.5. As such, these localized impingement effects may decrease the values of n [6].

For each of the n-paraffins studied here, the cooling crystallization function $K(T)$ was evaluated using an average value of the corresponding Avrami exponents in conjunction with eqn. (3). A plot of these cooling crystallization curves is given in Fig. 9. It is evident from such results that $K(T)$ decreases exponentially with increasing temperature which is typical of the overall crystallization rate for isothermal crystallization.

The validity of eqn. (18) is demonstrated in Fig. 10. Here, the results are plotted as $\ln[\Psi^*(T)]$ versus $1/T(\Delta T)^2$. The strong linearity of the plots in Fig. 10 confirm the applicability of eqn. (18). The corresponding values of the intercepts, $\ln(C_1)$, and the slopes, C_2, are summarized in Table 4.

Non-isothermal DSC thermograms have been used in the past to give reasonable estimates of the surface free energies [11, 26]. Here, values of $\sigma^2\sigma_e$ can be extracted from the values of C_2 using the relation

$$C_2 = \frac{8\pi\sigma_e\sigma^2(T_m^\circ)^2}{\kappa(\Delta H_f)^2} \tag{20}$$

TABLE 4

Parameters $\ln(C_1)$ and C_2 in eqn. (18) for the different n-paraffins

Compound	n	$\ln(C_1)$	$C_2 \times 10^{-4}(K^3)$	ΔH_f (J g^{-1})	σ (mJ m^{-2})
n-$C_{30}H_{62}$	2.3	−2.07	1.57	264.3	5.2
n-$C_{34}H_{70}$	2.6	−1.21	1.30	267.8	4.7
n-$C_{44}H_{90}$	2.2	−2.30	1.71	273.6	5.4
n-$C_{50}H_{102}$	3.0	−0.92	1.39	276.0	4.8

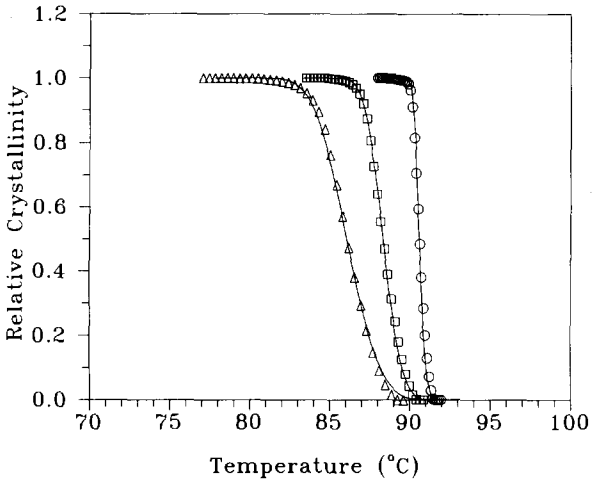

Fig. 11. Modelling the non-isothermal crystallization for n-$C_{50}H_{102}$ at different cooling rates: ○, 1°C min^{-1}; □, 5°C min^{-1}; △, 10°C min^{-1}; ——, model.

where the ΔH_f values for 100% crystalline n-paraffins are estimated using the thermodynamic equation of Dollhopf et al. [27]. Using Hoffman's estimated value of $\sigma_e = 0.17$ mJ m^{-2} for pure n-$C_{94}H_{190}$ [13], the lateral surface free energies were found to be approx. 5 mJ m^{-2} on average, with no systematic variation with carbon number (see Table 4). This behaviour is in good agreement with earlier findings [11, 13, 21] where it was concluded that σ for the n-paraffins with chain length longer than n-$C_{15}H_{32}$, does not change markedly with chain length or morphology.

The values of σ obtained in this study are relatively lower than those of

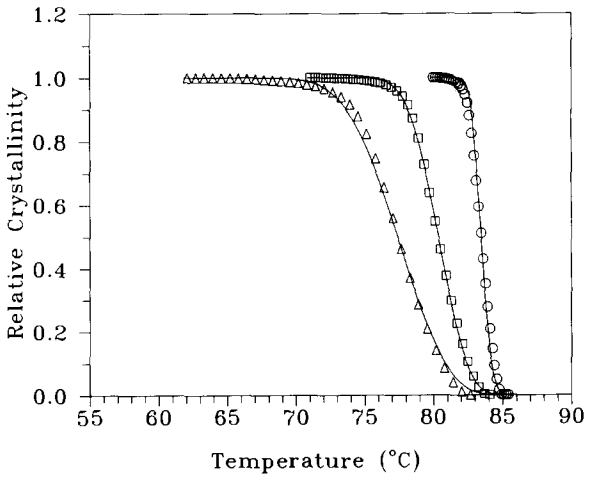

Fig. 12. Modelling the non-isothermal crystallization for n-$C_{44}H_{90}$ at different cooling rates (symbols as in Fig. 11).

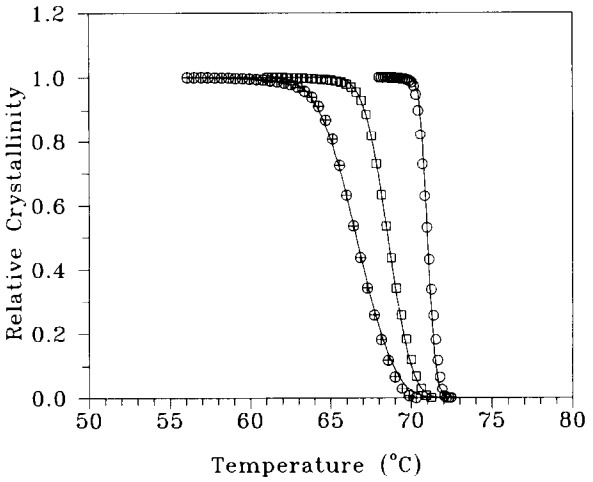

Fig. 13. Modelling the non-isothermal crystallization for n-$C_{34}H_{70}$ at different cooling rates: ○, 1°C min^{-1}; □, 5°C min^{-1}; ⊕, 9°C min^{-1}; ——, model.

Oliver and Calvert [11]. It is possible, however, that these parameters are sensitive to the approach used to analyse DSC thermograms. For instance, Oliver and Calvert [11] have shown that homogeneous nucleation data in the range n-$C_{16}H_{34}$–n-$C_{28}H_{58}$ give $\sigma = 6.6 \pm 1.3$ mJ m^{-2} when DSC thermograms are analysed according to their approach; consistently 25% lower values of σ were obtained when the same DSC curves were treated using the procedure of Cormia et al. [26]. Therefore, we believe that the values of σ are sensitive to the cooling rates i.e. the experimental conditions, and/or the actual nucleation behaviour. As a matter of fact,

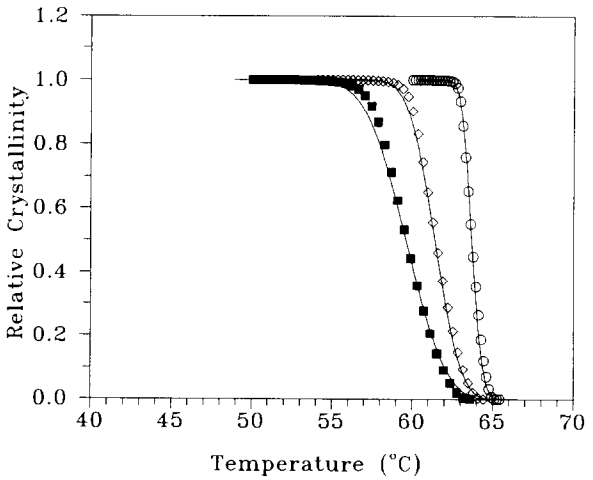

Fig. 14. Modelling the non-isothermal crystallization for n-$C_{30}H_{62}$ at different cooling rates: ○, 1°C min^{-1}; ◇, 4°C min^{-1}; ■, 7°C min^{-1}; ——, model.

Turnbull and Cormia [28] considered the possibility of nucleation occurring at the surface of the specimen rather than within its volume. They concluded that only volume nucleation would give reasonable agreement with time dependence of nucleation rate in isothermal experiments. Obviously, this may not be true for non-isothermal crystallization, especially at high cooling rates.

The adequacy of the present model can be tested further by predicting the non-isothermal data using the parameters in Table 4. As depicted in Figs. 11–14, the model predictions do indeed compare favourably with the experimental data for all four n-paraffins studied here. However, as mentioned previously, this model is applicable only at relatively low degrees of supercooling; its validity at high cooling rates, which correspond to high ΔT values, remains to be verified experimentally.

CONCLUSIONS

The Ozawa theory was shown to be a good technique for analysing non-isothermal crystallization data of four even-number n-paraffins. The experimental data of the studied n-paraffins followed eqn. (2) quite accurately, enabling the determination of the Avrami exponent. The proposed formulation of the Ozawa cooling crystallization function allowed reasonable estimates of the lateral surface free energies which agreed, within experimental error, with the literature. This simple model was deemed a success as it yielded excellent qualitative as well as quantitative predictions of the non-isothermal data.

ACKNOWLEDGEMENTS

Financial support was provided by the Natural Sciences and Engineering Research Council (NSERC) of Canada and the Department of Chemical and Petroleum Engineering (University of Calgary).

REFERENCES

1 S.M. Bucaram, J. Pet. Technol., 19 (1967) 150.
2 T. Ozawa, Polymer, 12 (1971) 150.
3 M. Avrami, J. Chem. Phys., 7 (1939) 1103.
4 U.R. Evans, Trans. Faraday Soc., 41 (1945) 365.
5 H. Elias, Macromolecules, Vol. 1, Plenum Press, New York, 1977, p. 393.
6 L.C. López and G.L. Wilkes, Polymer, 30 (1989) 882.
7 G. Ungar, J. Stejny and A. Keller, Science, 229 (1985) 386.
8 M. Chichalki and F.W. Jessen, Ind. Eng. Chem., 59 (1967) 86.
9 I. Bidd and M.C. Whiting, J. Chem. Soc. Chem. Commun., (1985) 543.
10 D. Turnbull and J.C. Fisher, J. Chem. Phys., 17 (1949) 71.
11 M.J. Oliver and P.D. Calvert, J. Crystal Growth, 30 (1975) 343.
12 D. Turnbull and F. Spaepen, J. Polym. Sci. Polym. Symp., 63 (1978) 237.
13 J.D. Hoffman, Macromolecules, 18 (1985) 772.

14 R.L. Cormia, F.P. Price and D. Turnbull, J. Chem. Phys., 37 (1962) 1333.
15 C.F. Pratt and S.Y. Hobbs, Polymer, 17 (1976) 12.
16 A. Hammami, MS Thesis, University of Tennessee, Knoxville, 1990.
17 P.J. Phillips and R.A. Campbell, personal communication, University of Tennessee, Knoxville, 1990.
18 C.G. Gray, J. Inst. Petrol., 29 (1943) 226.
19 W.M. Mazee, Recl. Trav. Chim., 67 (1948) 197.
20 A.A. Schaerer, C.J. Busso, A.E. Smith and L.B. Skinner, J. Am. Chem. Soc., 77 (1955) 2017.
21 A.A. Schearer, G.G. Baylé and W.M. Mazee, Revl. Trav. Chim., 75 (1956) 513.
22 W.H. Carothers, J.W. Hill, J.E. Kirby and R.A. Jacobson, J. Am. Chem. Soc., 52 (1930) 5279.
23 E.W. Clarke, Ind. Eng. Chem., 43 (1951) 2526.
24 B. Hubbard, Am. Mineral., 30 (1945) 645.
25 W.R. Turner, Ind. Eng. Chem. Prod. Res. Dev., 10 (1971) 238.
26 R.L. Cormia, F.P. Price and D. Turnbull, J. Chem. Phys., 37 (1962) 1333.
27 W. Dollhopf, H.P. Grossmann and U. Leute, Colloid Polym. Sci., 259 (1981) 267.
28 D. Turnbull and R.L. Cormia, J. Chem. Phys., 34 (1961) 820.